Robust Wave Splitters Based on Scattering Singularities in Complex non-Hermitian Systems

Jared Erb,[1, a)] Nadav Shaibe,[1] Tsampikos Kottos,[2] and Steven M. Anlage[1]
[1)]*Maryland Quantum Materials Center, Department of Physics, University of Maryland, College Park, MD, 20742, USA*
[2)]*Wave Transport in Complex Systems Lab, Physics Department, Wesleyan University, Middletown, CT, 06459, USA*

(Dated: 10 November 2025)

We have discovered specific conditions for generic scattering systems to act as wave splitters that are robust to any change in relative amplitude or phase of an arbitrary injected waveform. Specifically for complex systems with tunable parameters, these conditions for robust splitting (RS) are abundant, and by using multiple tunable parameters the relative amplitude and phase of the output signals can also be tuned. The splitting property of the systems works for all possible input phase differences and amplitude ratios and does not require a particular coherent input signal. We show experimentally that the fixed splitting ratios and output phases at RS conditions are robust to 100 dB of relative power and 2π phase changes of the input waves to a complex non-Hermitian two-port system. We also demonstrate that the splitting power ratio can be tuned by multiple orders of magnitude and the RS conditions can be tuned to any desired frequency with suitable tunable perturbations embedded in the system. Although this phenomenon is realized in two-port systems and involves some degree of attenuation, tunable robust splitting can be achieved between any two ports of multiport systems. These results are general to all wave scattering phenomena (electromagnetic, acoustic, etc.) and hold in generic complex scattering systems.

Coherent Perfect Absorption (CPA) is a remarkable phenomenon where in a lossy system, injected electromagnetic radiation is completely absorbed, such that no incident energy leaves the system through reflection or transmission. This phenomenon was first discovered in the context of time-reversed lasers[1–3]. Under this condition, a system acts as a lossy resonant cavity where a coherent excitation, corresponding to the scattering matrix eigenvector associated with the zero eigenvalue, results in perfect absorption. This has attracted much attention for its potential applications, including sensing[4–6], photodetection[7–9], filtering[10,11], communication[12–16], wireless power transfer[17], wavefront shaping[18,19], broadband absorption[20–22], etc. These applications can be implemented in any wave-scattering system, as demonstrated by studies of CPA using Random Matrix Theory (RMT) models of generic scattering systems[23,24].

In the past, CPA was most commonly demonstrated in systems that are highly symmetric. In contrast, more recent work has shown that generic multi-modal cavities with or without reciprocity can be manipulated to create the conditions needed for CPA's at arbitrary frequencies[15,16,18,19,25–31]. Inspired by foundational work on CPA, and newer work expanding applications of CPA to generic complex scattering systems, we now recognize that the conditions required to display CPA also present an opportunity for another phenomenon, which we term "robust splitting" (RS). We demonstrate that at these conditions, any signal sent into the system will be output with a particular fixed relative amplitude and phase (albeit with some overall attenuation) which depend on system-specific details. In the limiting case that the CPA waveform is injected, then the signal is perfectly absorbed.

[a)]Corresponding author: jmerb@umd.edu

One of the key features in the newer works on creating the conditions required for CPA, compared to previous ones, is the implementation of electronically-controlled tunable parameters embedded within a system. These tunable parameters allow for a more thorough manipulation of the scattering singularities of a system, including RS conditions, and their dynamics. Due to the topological protection of the scattering singularities, along with the ease of finding and manipulating them with tunable parameters, the potential to find applications of these singularities is greatly increased.

In this paper, we show experimentally and theoretically that for all arbitrary monochromatic signals injected into a two-port system set to RS conditions (excluding the CPA waveform corresponding to the zero eigenvalue), using one port or both ports simultaneously, the output signals will have a robust relative amplitude and phase. Additionally, due to the topological stability and manipulability of RS conditions, the values of the relative amplitude and phase can be continuously varied by tuning a third parameter of the system. We also demonstrate the combined case of RS conditions and a scattering matrix exceptional point degeneracy in a non-reciprocal system.

To demonstrate the generality of robust splitting conditions, we employ complex multi-modal physical systems interrogated by $M = 2$ scattering channels. These systems are characterized by a 2×2 scattering matrix S which relates the incoming and outgoing wave excitations for each channel:

$$\begin{pmatrix} V_1^{\text{out}} \\ V_2^{\text{out}} \end{pmatrix} = S \begin{pmatrix} V_1^{\text{in}} \\ V_2^{\text{in}} \end{pmatrix}, \tag{1}$$

where $V_n^{\text{in}}, V_n^{\text{out}}$ are the complex voltages of the incoming and outgoing excitations on channel $n = 1, 2$ respectively. The scattering matrix is experimentally measured in the frequency domain using a Keysight model N5242B microwave vector

network analyzer (VNA) connected to two channels of the systems using coaxial cables. Due to the lossiness of the physical systems, S is sub-unitary, and due to the underlying complex (chaotic) ray dynamics its complex matrix elements are irregular functions of frequency.

The systems used in this work are quasi-one-dimensional microwave graphs (reciprocal and non-reciprocal)[32–36], a quasi-two-dimensional microwave billiard[37–42], and a three-dimensional microwave cavity[25,43–45] (see insets (i-iii) of Figure 2). To exert control over the scattering properties, each system contains electronically-controlled metasurfaces or phase-shifters which modify the amplitude and phase of reflecting and/or propagating waves. These tunable devices are denoted as TM_p^{qD}, where q indicates the dimension of the device ($q=0$ for phase shifters and $q=1,2$ for the one and two-dimensional metasurfaces) and $p=1,2,3,...$ labels each device within a system. The number of tunable devices in each experimental system was determined by the number available, but in general two tunable devices are enough to achieve all the results shown in this paper. However, the more tunable devices in use, the easier it is to accomplish any specific condition. The metasurfaces used in this work are tuned by a global voltage bias which modulates the amplitude and phase of reflected waves[28,31,46]. For additional details on the measurements and experimental systems used, see supplementary material I and Ref. 31. Embedding tunable devices in the systems allows for multi-dimensional parametric variation of the scattering matrix and its singularities, including robust splitting conditions. This capability enables us to find numerous scattering singularities which we can manipulate and utilize for applications.

To identify scattering singularities in a multi-dimensional parameter space, we use conditions of the scattering matrix that correspond to each singularity. For robust splitting conditions in particular, an eigenvalue of the scattering matrix is zero. A zero eigenvalue also corresponds to the zero of the determinant, as at least one eigenvalue of S must be $0+i0$ for $det(S)$ to equal $0+i0$. In practice, the conditions for identifying singularities incorporate a tolerance for purposes of visualization.

An abundance of singularities, specifically points of RS conditions (corresponding to $det(S)=0+i0$), can be seen in Figure 1 where $|det(S)|$ is plotted vs frequency and phase shift of TM_1^{0D} measured in a non-reciprocal tetrahedral microwave graph. We have identified 26 RS conditions marked by white triangles. Numerous RS conditions are seen in many types of generic wave-scattering systems with or without reciprocity (see Figs. S1, S2 in supplementary material II).

Using the 2-port dual-source mode of the VNA, we can directly inject arbitrary monochromatic signals into a system using one port or both ports simultaneously. When injecting a signal, the input and output power ratios $\left(\frac{P_1}{P_2}=\frac{|V_1|^2}{|V_2|^2}\right)$ and phase difference between the ports are systematically varied and measured. From this, we can determine the unique properties of RS conditions once we have found their locations in parameter space. Except in the case of exceptional point degeneracies, which is described later and in more detail in

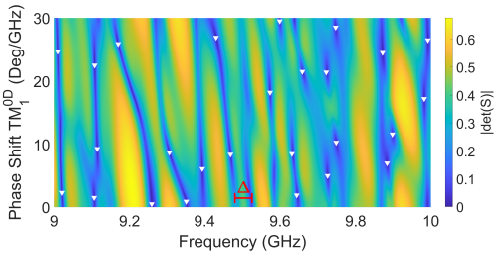

FIG. 1. Plot of $|det(S)|$ vs frequency and phase shift of TM_1^{0D} in the non-reciprocal tetrahedral microwave graph. The white triangles correspond to points where $det(S)=0+i0$, which enable robust splitting. The mean mode spacing ($\Delta=\frac{c}{2L}$) of the graph is approximately 45 MHz, and is marked in red near the bottom of the plot.

supplementary material III, any signal sent to, and returned from, an arbitrary two-port scattering system can be written as a linear combination of the two S-matrix eigenvectors:

$$\begin{pmatrix} V_1^{\text{in}} \\ V_2^{\text{in}} \end{pmatrix} = c_1 |R_1\rangle + c_2 |R_2\rangle \tag{2}$$

$$\begin{pmatrix} V_1^{\text{out}} \\ V_2^{\text{out}} \end{pmatrix} = S \begin{pmatrix} V_1^{\text{in}} \\ V_2^{\text{in}} \end{pmatrix} = c_1 \lambda_S^{(1)} |R_1\rangle + c_2 \lambda_S^{(2)} |R_2\rangle , \tag{3}$$

where $\begin{pmatrix} V_1^{\text{in}} \\ V_2^{\text{in}} \end{pmatrix}$, $\begin{pmatrix} V_1^{\text{out}} \\ V_2^{\text{out}} \end{pmatrix}$ are the input and output signals respectively, $|R_{1,2}\rangle$ are the right eigenvectors of the sub-unitary scattering matrix S, $c_{1,2}$ are arbitrary coefficients, and $\lambda_S^{(1,2)}$ are the corresponding eigenvalues, which are complex in general.

If the system is set to RS conditions (without loss of generality, let $\lambda_S^{(1)}=0+i0$),

$$\begin{pmatrix} V_1^{\text{out}} \\ V_2^{\text{out}} \end{pmatrix} = c_2 \lambda_S^{(2)} |R_2\rangle . \tag{4}$$

Therefore, for any arbitrary monochromatic signals sent into the system, the relative amplitude and phase of the output signals are robust and determined by $|R_2\rangle$ (excluding the set of measure zero where $c_1=1$, $c_2=0$, which is the conventional CPA injection[19,28]). The contribution of the eigenvector corresponding to the zero eigenvalue of the input signal is completely absorbed by the system. The overall amount of signal that is absorbed after injection is dependent on both the proportion of the input signal on $c_1|R_1\rangle$ and the value of $\lambda_S^{(2)}$. For systems with less overall loss, $|\lambda_S^{(2)}|$ will tend to be closer to unity and the output signal will have more power. Additional discussion of signal loss is described in supplementary material IV. In practice, once the RS condition has been found, the robust splitting value that the output signal obeys can be indirectly determined from the relative amplitude and phase

of the two components of the scattering matrix eigenvector corresponding to the non-zero eigenvalue (see supplementary material V for the analytic form of the eigenvectors at RS conditions). This eigenvector depends on the scattering matrix elements, so in general at different RS conditions, the output power ratio and phase difference will also be different.

To directly determine the robust splitting ratio of RS conditions, we inject signals over a large range of channel amplitudes and relative phases. In Figure 2, we experimentally demonstrate that the power ratio and phase difference of the output signals at an RS condition are robust to 100 dB of relative power and 2π phase change of the input signal. Note, for input power ratios $|P_1^{in}/P_2^{in}| \geq 40$ dB, this is effectively a single port excitation. In this figure, for the specific RS condition measured, the amplitude and phase of the output signals are fixed at approximately 3.85 and -128.8 degrees respectively, independent of the value of the input signals.

To show that different RS conditions have different splitting ratios, we found 28 unique RS conditions in all four of the physical systems described above, and show the results in Figure 3. In this figure, we show the output power ratio and phase difference vs the input power ratio and input phase difference for all 28 RS conditions measured. The color of the curve corresponds to the specific system measured (black: reciprocal graph, red: non-reciprocal graph, blue: two-dimensional billiard, green: three-dimensional cavity). The solid curves correspond to measurements where the power at port 1 was less than the power at port 2, and vice versa for the dashed curves. We see that nearly all curves are flat, proving the robustness of the output signals at RS conditions. The green curves from the three-dimensional cavity are the least flat because during the time it takes to find the RS conditions and inject the input signals, the environment of the system can change, causing the system to drift away from the RS conditions. See Figure S7 in supplementary material VI to see signal injection in systems not set to RS conditions. In contrast with the robustness of the output signals at RS conditions, output signals away from RS conditions vary significantly as the input signals change.

If we slowly vary the value of a third tunable parameter while measuring the scattering matrix over the same two-dimensional parameter space, such as the one shown in Fig. 1, we can continuously manipulate the location of the singularities of the scattering matrix[31] (see supplementary material VII for a video showing the dynamics of RS conditions). Within the two-dimensional parameter space, as the third parameter varies, the scattering singularities are topologically stable except in certain instances when they are created or annihilated in pairs. For RS conditions in particular, as their locations move in parameter space, their robust splitting values also vary. This is shown in Figure 4, where the left plot shows the location of an RS condition moving in the frequency and phase shift of TM_1^{0D} parameter space as the phase shift of TM_2^{0D} is varied. The right plots show how the output power ratio and phase difference vary along the trajectory of the evolving RS condition. The colors show the continuous evolution of the third parameter, phase shift of TM_2^{0D}. For this RS condition, the output power ratio varies by multiple orders of magnitude and the output phase difference varies over 260 degrees. Similar examples obtained in the two-dimensional quarter bow-tie billiard and the three-dimensional microwave cavity are shown in Figs. S3, S4. Due to the complexity of our experimental systems, any perturbation to the system will affect the scattering properties, which also affects the location of the RS conditions as well as their output power ratio and phase difference. To view the stability of RS conditions over time in a one- and two-dimensional system see Figs. S9, S10 in supplementary material VIII.

We have established that utilizing a single tunable parameter and frequency we can find an abundance of scattering singularities. However, within each of the physical systems, there are multiple phase shifters or metasurfaces which can be used to perturb the system. Using these multiple tunable parameters, we can do more advanced manipulation of the scattering singularities, such as combining them at a single location in a two-dimensional parameter space. A particularly interesting combination case is that of an exceptional point degeneracy (EPD) and a robust splitting condition. At an exceptional point degeneracy, both the scattering matrix eigenvalues and associated eigenvectors become degenerate[47–52]. In prior work, the CPA and EPD combination has been shown in the spectrum of the Hamiltonian[53–55] and the RS condition and EPD combination has been shown in the scattering matrix of a reciprocal scattering system[31]. In Figure 5, we demonstrate an RS+EPD combination in a non-reciprocal system. In this figure, we show that both scattering eigenvalues are near $\lambda_S = 0 + i0$, and that the output signal power ratio and phase difference are robust to changes in the input signal power ratio and phase difference. The results show small deviations from ideal flatness because the scattering eigenvalues $|\lambda_S^{(1)}| + |\lambda_S^{(2)}| = 0.029 \neq 0$. As this was measured in a non-reciprocal system, the combined case of RS conditions and EPD is no longer a 50:50 power splitter, as predicted for reciprocal systems in Ref. 31. The output power ratio and phase difference can take any value in non-reciprocal systems, as can be seen from the analytic formula for the degenerate eigenvector at RS and EPD conditions: $|R_{RS+EPD}\rangle \propto \begin{pmatrix} \frac{-S_{22}}{S_{21}} \\ 1 \end{pmatrix}$ (see supplementary material III for additional details on the RS and EPD combination). For each instance of an RS+EPD combination in a non-reciprocal system, the value of $\frac{-S_{22}}{S_{21}}$ (magnitude and phase) fixes the output power ratio and phase difference, but different instances of RS+EPD combinations will have different values of $\frac{-S_{22}}{S_{21}}$. In addition, since the RS conditions and EPD's are independent singularities, in general any perturbation to the system will split the combination apart.

All of the above results are generic to all complex wave-scattering systems. To confirm this, we utilize a Random Matrix Theory model (see supplementary material IX, X), which have been well established in the literature to describe the universal scattering properties of generic complex resonant systems[56–66]. In Figure S11, similar to Figure 1, the $|det(S)|$ is plotted vs ω and parameter x, where ω is the frequency and parameter x is a surrogate for the tunable metasurface. There are 21 RS conditions marked by white triangles. In Figure

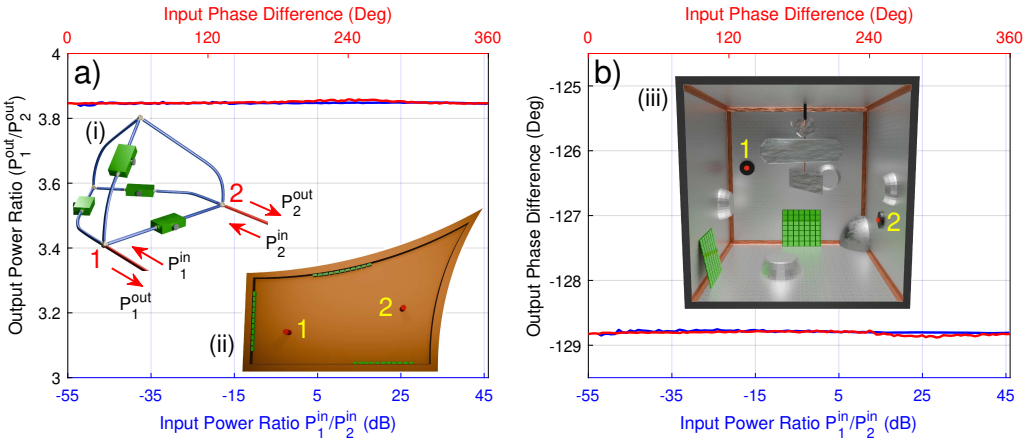

FIG. 2. Experimental demonstration of the robust splitting conditions in the quarter bow-tie two-dimensional billiard and schematics of three experimental systems. (a) Output power ratio vs input power ratio (lower axis, blue) and input phase difference (upper axis, red). The blue curve corresponds to the input signals power ratio being swept at a fixed phase difference, and the red curve corresponds to the input signals relative phase being swept at a fixed power ratio. Left inset (i) depicts a schematic view of a quasi-one-dimensional tetrahedral microwave graph with phase shifters ($TM^{0D}_{p=1,2,3,4}$) along four of the bonds. The ports connected to the graph are indicated by the red cables and numbers. The arrows indicate the input and output signals to/from the graph. Right inset (ii) depicts a schematic view of a quarter bow-tie two-dimensional billiard with three one-dimensional metasurfaces ($TM^{1D}_{p=1,2,3}$) along the walls of the billiard. The ports connected to the billiard are indicated by the red cylinders and yellow numbers. (b) Output phase difference vs input power ratio (lower axis, blue) and input phase difference (upper axis, red). The blue and red curves have the same interpretation as in (a). Inset (iii) depicts a schematic view of a three-dimensional microwave cavity with two two-dimensional metasurfaces ($TM^{2D}_{p=1,2}$) along the walls of the cavity. The ports connected to the cavity are indicated by the red cylinders and yellow numbers.

S12, similar to Figure 4, we see that the location of an RS condition can be strongly manipulated in a two-dimensional parameter space by means of a third parameter (in this case parameter y, which acts similarly to x), and the output power ratio and phase difference vary significantly.

In conventional RF and microwave settings, there are several passive devices that act as a wave splitter. These devices include power splitters, directional couplers, hybrid couplers, etc[67]. Most commonly, these devices take the form of a three- or four-port network, with the input ports being distinct from the output ports. Examples of power splitters are T-junctions and Wilkinson power dividers[68]. Generally, power splitters take an input signal and split it into two output signals with equal amplitude and phase, although it's possible for output signals to be split into N channels with an unequal power split. Directional couplers can be designed for an arbitrary (but fixed) output power split, while hybrid couplers generally have an equal power split[67]. The 90° and 180° hybrid couplers take an input signal and split it into two equal amplitude signals with a 90° phase difference or either a 180° or 0° phase difference respectively.

In general, conventional wave splitters are networks (graphs) that take a single input signal and output $N \geq 2$ signals at some fixed amplitude and phase ratios, where the input and output ports are distinct. These splitters can be designed to work over a broad frequency band, but the output amplitudes and phases cannot be tuned. In contrast, we have shown that the RS phenomenon can convert any generic two-port complex scattering system with adjustable parameters into a *tunable* robust splitter. One should note that the output signals suffer a degree of net loss dependent on the value of the non-zero eigenvalue and the details of the input signal. In particular, as the input signals approach the CPA eigenvector, the degree of net loss increases until the signal is completely absorbed. If the input signals vary considerably, then the amount of net loss suffered can also vary substantially. In Fig. 6, we show surface plots of $\frac{P_{out}}{P_{in}}$ vs input power ratio and input phase difference of injected signals for two representative examples of RS conditions from the experimental reciprocal tetrahedral graph (for additional details about this figure and output signal loss in different systems see supplementary material IV). In this figure, we see that the locations of the CPA and "Anti-CPA" eigenvectors (white and red triangles, respectively) in the input signal power/phase parameter space determine the regions where the output signal has a significant, or minimal, amount of net loss. While there can be large regions of parameter space where there is a significant amount of net loss, for applications where the input signal values are known and don't vary too much, a system can be designed to have the minimal loss (near the "Anti-CPA" eigenvector, red triangle in Fig. 6) at those values. The net loss can be further reduced by designing the RS condition to have the non-zero eigenvalue

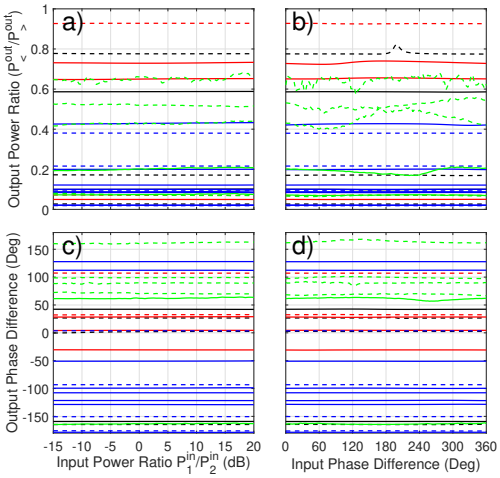

FIG. 3. Experimental demonstration of the robust splitting of 28 unique robust splitting conditions from four different experimental systems. The black curves were measured in a 1D reciprocal tetrahedral graph, red curves in a 1D non-reciprocal tetrahedral graph, blue curves in a 2D quarter bow-tie billiard, and green curves in a chaotic 3D microwave cavity. The dashed lines correspond to output power ratios where $P_1^{out} > P_2^{out}$ and solid lines correspond to $P_1^{out} < P_2^{out}$. (a) Output power ratio vs input power ratio. (b) Output power ratio vs input phase difference. (c) Output phase difference vs input power ratio. (d) Output phase difference vs input phase difference.

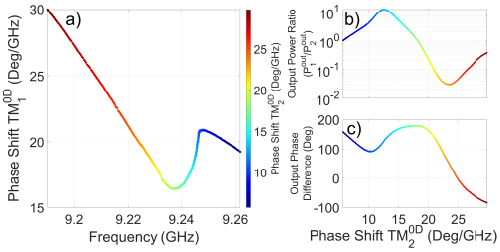

FIG. 4. Experimental demonstration of the continuous tunability of robust splitting conditions in the reciprocal tetrahedral microwave graph. The color of each point corresponds to the value of the varying third parameter of the system (TM_2^{0D}) the RS condition was measured at. (a) Location of an RS condition in the two-dimensional parameter space of frequency and phase shift of TM_1^{0D} as the phase shift of TM_2^{0D} varies. (b) Output power ratio vs phase shift of TM_2^{0D}. (c) Output phase difference vs phase shift of TM_2^{0D}.

of S near the unit circle, increasing $\frac{P_{out}}{P_{in}}$ to be nearly 1 at the location of the "Anti-CPA" eigenvector.

Additionally, this phenomenon only works at a single frequency at a time, but due to the abundance and manipulability of RS conditions, a tunable system can exhibit robust splitting at arbitrary frequencies. Another important distinction is that for RS conditions, the input ports and output ports are the same. The input signal can be injected into one or both ports, but the output signal will have a robust splitting value between both ports. Due to the directed nature of conventional splitters, there is usually unwanted reflection at the input port. However in the RS case, the input and output ports are identical, therefore the issue of unwanted reflection is irrelevant.

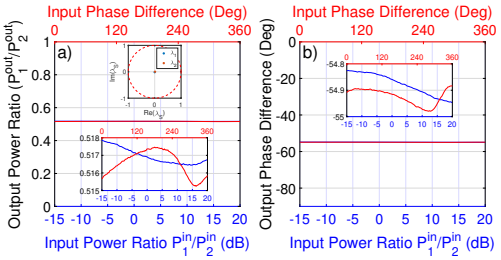

FIG. 5. Experimental demonstration of the robust splitting of RS+EPD in a non-reciprocal tetrahedral microwave graph. (a) Output power ratio vs input power ratio (lower axis, blue) and input phase difference (upper axis, red). The blue curves correspond to the input signals power ratio being swept, and the red curves correspond to the input signals relative phase being swept. Top inset shows the eigenvalues of the scattering matrix in the complex plane. Bottom inset shows a vertical zoom-in to illustrate the details of the curves. (b) Output phase difference vs input power ratio (lower axis, blue) and input phase difference (upper axis, red). The blue and red curves have the same interpretation as in (a). Inset shows a vertical zoom-in to magnify the details of the curves.

The results discussed in this work were obtained using a 2×2 scattering matrix, but can be generalized to higher dimensions. The conditions for $det(S) = 0 + i0$ are still abundant, topologically protected, and can be manipulated in higher dimensions as $det(S)$ remains a simple complex scalar function for any number of ports. Unfortunately, the robust splitting phenomenon only generically occurs when measuring a 2×2 scattering matrix (see supplementary material XI for details on signal injection in scattering systems with many ports). However, systems with multiple ports can still achieve robust splitting between any two ports by only injecting and receiving signals on those two ports, while also at RS conditions.

Instead of the conventional use of CPA to absorb all incident energy, we have discovered a way to use RS conditions to create robust splitters (albeit with a variable and sometimes substantial overall loss), and with multiple tunable parameters we can continuously change the relative amplitude and phase of the robust output signal. Using enough tunable parameters, a degree of control can be created over the output splitting values, including independent control of the output power ratio and phase difference. With the ability to generate and manipulate numerous scattering singularities, this provides an alternative to special design/engineering considerations to establish RS conditions at particular frequencies,

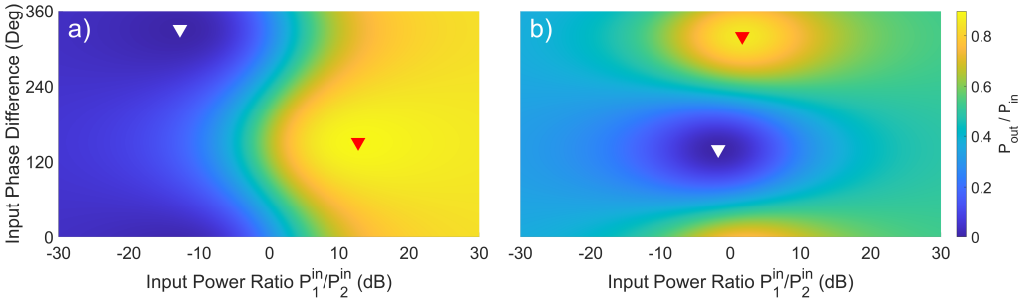

FIG. 6. Plots showing $\frac{P_{out}}{P_{in}}$ vs input power ratio P_1^{in}/P_2^{in} and input phase difference for representative examples of arbitrary signal injection into a reciprocal tetrahedral graph set to two different RS conditions. In each of the plots, the white triangle indicates the location of the coherent perfect absorption (CPA) eigenvector which corresponds to $\frac{P_{out}}{P_{in}} = 0$ and the red triangle indicates the location of the "Anti-CPA" eigenvector which corresponds to the maximal value of $\frac{P_{out}}{P_{in}}$.

since the tunable parameters take care of that problem. The topological protection of the RS conditions (as long as they are not annihilated with a separate RS condition), and their ease of manipulation, make applications of these singularities more feasible. Additionally, using the RMT model we have shown that these phenomena are general to all complex wave-scattering systems.

SUPPLEMENTARY MATERIAL

In the supplementary material, section I describes the experimental systems and procedures used in this work, section II demonstrates robust splitting (RS) phenomena in the experimental systems not shown in the main text, section III describes exceptional point degeneracy (EPD) phenomena and how it affects signal injection, section IV discusses the overall loss associated with signals injected at RS conditions, section V gives the general analytic form of the eigenvectors and their simplified forms at RS conditions, section VI shows signal injection into systems not at RS conditions, section VII contains a movie of the dynamics of RS conditions, section VIII discusses the stability over time of systems set to RS conditions, section IX details the Random Matrix Theory (RMT) model of complex scattering systems used in this work, section X shows results of the RMT model that have the same features as the experimental results, and section XI generalizes signal injection and EPD's for higher dimensional scattering matrices.

ACKNOWLEDGMENTS

This work was partially supported by NSF/RINGS under grant No. ECCS-2148318, ONR under grant N000142312507, DARPA WARDEN under grant HR00112120021, Department of Energy under grant DE-SC0024223, and US-Israel Binational Science Foundation under grant BSF2022158.

DATA AVAILABILITY STATEMENT

The data that support the findings of this study are openly available in the Digital Repository at the University of Maryland at https://doi.org/10.13016/lxva-rkcs.

[1] Y. D. Chong, L. Ge, H. Cao, and A. D. Stone, Physical Review Letters **105**, 053901 (2010).
[2] W. Wan, Y. Chong, L. Ge, H. Noh, A. D. Stone, and H. Cao, Science **331**, 889 (2011).
[3] D. G. Baranov, A. Krasnok, T. Shegai, A. Alù, and Y. Chong, Nature Reviews Materials **2**, 17064 (2017).
[4] S. Dutta-Gupta, O. J. F. Martin, S. D. Gupta, and G. S. Agarwal, Opt. Express **20**, 1330 (2012).
[5] J. Zhang, C. Guo, K. Liu, Z. Zhu, W. Ye, X. Yuan, and S. Qin, Opt. Express **22**, 12524 (2014).
[6] C. Meng, X. Zhang, S. T. Tang, M. Yang, and Z. Yang, Scientific Reports **7**, 43574 (2017).
[7] T. Roger, S. Vezzoli, E. Bolduc, J. Valente, J. J. F. Heitz, J. Jeffers, C. Soci, J. Leach, C. Couteau, N. I. Zheludev, and D. Faccio, Nature Communications **6**, 7031 (2015).
[8] A. N. Vetlugin, Phys. Rev. A **104**, 013716 (2021).
[9] A. N. Vetlugin, F. Martinelli, S. Dong, and C. Soci, Nanophotonics **12**, 505 (2023).
[10] J. Zhang, K. F. MacDonald, and N. I. Zheludev, Light: Science & Applications **1**, e18 (2012).
[11] F. T. Faul, L. Cronier, A. Alhulaymi, A. D. Stone, and P. del Hougne, Advanced Science **12**, 2500796 (2025).
[12] R. Bruck and O. L. Muskens, Opt. Express **21**, 27652 (2013).
[13] Y. Sun, W. Tan, H.-q. Li, J. Li, and H. Chen, Phys. Rev. Lett. **112**, 143903 (2014).
[14] Z. J. Wong, Y.-L. Xu, J. Kim, K. O'Brien, Y. Wang, L. Feng, and X. Zhang, Nature Photonics **10**, 796 (2016).
[15] M. F. Imani, D. R. Smith, and P. del Hougne, Advanced Functional Materials **30**, 2005310 (2020).
[16] P. del Hougne, K. B. Yeo, P. Besnier, and M. Davy, Phys. Rev. Lett. **126**, 193903 (2021).
[17] A. Krasnok, D. G. Baranov, A. Generalov, S. Li, and A. Alù, Phys. Rev. Lett. **120**, 143901 (2018).
[18] K. Pichler, M. Kühmayer, J. Böhm, A. Brandstötter, P. Ambichl, U. Kuhl, and S. Rotter, Nature **567**, 351 (2019).
[19] L. Chen, T. Kottos, and S. M. Anlage, Nature Communications **11**, 5826 (2020).
[20] M. Pu, Q. Feng, M. Wang, C. Hu, C. Huang, X. Ma, Z. Zhao, C. Wang, and X. Luo, Opt. Express **20**, 2246 (2012).
[21] J. Z. Song, P. Bai, Z. H. Hang, and Y. Lai, New Journal of Physics **16**, 033026 (2014).
[22] S. Suwunnarat, Y. Tang, M. Reisner, F. Mortessagne, U. Kuhl, and T. Kottos, Communications Physics **5**, 5 (2022).
[23] H. Li, S. Suwunnarat, R. Fleischmann, H. Schanz, and T. Kottos, Phys. Rev. Lett. **118**, 044101 (2017).
[24] Y. V. Fyodorov, S. Suwunnarat, and T. Kottos, Journal of Physics A: Mathematical and Theoretical **50**, 30LT01 (2017).
[25] B. W. Frazier, T. M. Antonsen, S. M. Anlage, and E. Ott, Physical Review Research **2**, 043422 (2020).
[26] P. del Hougne, K. B. Yeo, P. Besnier, and M. Davy, Laser & Photonics Reviews **15**, 2000471 (2021).
[27] L. Chen, S. M. Anlage, and Y. V. Fyodorov, Phys. Rev. E **103**, L050203 (2021).
[28] J. Erb, D. Shrekenhamer, T. Sleasman, T. M. Antonsen, and S. M. Anlage, Acta Physica Polonica A **144**, 421 (2024).
[29] C.-Z. Wang, J. Guillamon, W. Tuxbury, U. Kuhl, and T. Kottos, Phys. Rev. Appl. **22**, 064093 (2024).
[30] N. Shaibe, J. M. Erb, and S. M. Anlage, Phys. Rev. Lett. **134**, 147203 (2025).
[31] J. Erb, N. Shaibe, R. Calvo, D. P. Lathrop, T. M. Antonsen, T. Kottos, and S. M. Anlage, Phys. Rev. Res. **7**, 023090 (2025).
[32] T. Kottos and U. Smilansky, Phys. Rev. Lett. **79**, 4794 (1997).
[33] T. Kottos and U. Smilansky, Phys. Rev. Lett. **85**, 968 (2000).
[34] T. Kottos and U. Smilansky, Journal of Physics A: Mathematical and General **36**, 3501 (2003).
[35] O. Hul, S. Bauch, P. Pakoński, N. Savytskyy, K. Życzkowski, and L. Sirko, Phys. Rev. E **69**, 056205 (2004).
[36] M. Ławniczak, S. Bauch, O. Hul, and L. Sirko, Phys. Rev. E **81**, 046204 (2010).
[37] H.-J. Stöckmann and J. Stein, Phys. Rev. Lett. **64**, 2215 (1990).
[38] E. Doron, U. Smilansky, and A. Frenkel, Phys. Rev. Lett. **65**, 3072 (1990).
[39] P. So, S. M. Anlage, E. Ott, and R. N. Oerter, Phys. Rev. Lett. **74**, 2662 (1995).
[40] A. Gokirmak, D. H. Wu, J. S. A. Bridgewater, and S. M. Anlage, Review of Scientific Instruments **69**, 3410 (1998).
[41] Y. Hlushchuk, A. Kohler, S. Bauch, L. Sirko, R. Blümel, M. Barth, and H.-J. Stöckmann, Phys. Rev. E **61**, 366 (2000).
[42] B. Dietz, T. Friedrich, H. L. Harney, M. Miski-Oglu, A. Richter, F. Schäfer, and H. A. Weidenmüller, Phys. Rev. Lett. **98**, 074103 (2007).
[43] S. Deus, P. M. Koch, and L. Sirko, Phys. Rev. E **52**, 1146 (1995).
[44] H. Alt, C. Dembowski, H. D. Graf, R. Hofferbert, H. Rehfeld, A. Richter, R. Schuhmann, and T. Weiland, Physical Review Letters **79**, 1026 (1997).
[45] B. W. Frazier, T. M. Antonsen, S. M. Anlage, and E. Ott, Phys. Rev. Appl. **17**, 024027 (2022).
[46] T. Sleasman, R. Duggan, R. S. Awadallah, and D. Shrekenhamer, Phys. Rev. Appl. **20**, 014004 (2023).
[47] C. Dembowski, H.-D. Gräf, H. L. Harney, A. Heine, W. D. Heiss, H. Rehfeld, and A. Richter, Phys. Rev. Lett. **86**, 787 (2001).
[48] M. V. Berry, Czechoslovak Journal of Physics **54**, 1039 (2004).
[49] S.-Y. Lee, J.-W. Ryu, J.-B. Shim, S.-B. Lee, S. W. Kim, and K. An, Phys. Rev. A **78**, 015805 (2008).
[50] J. Wiersig, Phys. Rev. Lett. **112**, 203901 (2014).
[51] M.-A. Miri and A. Alù, Science **363**, eaar7709 (2019).
[52] Ş. K. Özdemir, S. Rotter, F. Nori, and L. Yang, Nature Materials **18**, 783 (2019).
[53] W. R. Sweeney, C. W. Hsu, S. Rotter, and A. D. Stone, Phys. Rev. Lett. **122**, 093901 (2019).
[54] C. Wang, W. R. Sweeney, A. D. Stone, and L. Yang, Science **373**, 1261 (2021).
[55] A. Farhi, A. Mekawy, A. Alù, and D. Stone, Physical Review A **106**, L031503 (2022).
[56] L. Couchman, E. Ott, and T. M. Antonsen, Phys. Rev. A **46**, 6193 (1992).
[57] Y. V. Fyodorov and H.-J. Sommers, Journal of Mathematical Physics **38**, 1918 (1997).
[58] C. W. J. Beenakker, Rev. Mod. Phys. **69**, 731 (1997).
[59] R. A. Méndez-Sánchez, U. Kuhl, M. Barth, C. H. Lewenkopf, and H.-J. Stöckmann, Phys. Rev. Lett. **91**, 174102 (2003).
[60] Y. V. Fyodorov and D. V. Savin, Journal of Experimental and Theoretical Physics Letters **80**, 725 (2004).
[61] U. Kuhl, M. Martínez-Mares, R. A. Méndez-Sánchez, and H.-J. Stöckmann, Phys. Rev. Lett. **94**, 144101 (2005).
[62] Y. V. Fyodorov and D. V. Savin, in *The Oxford Handbook of Random Matrix Theory*, edited by G. Akemann, J. Baik, and P. D. Francesco (Oxford University Press, 2011) pp. 703–722.
[63] U. Kuhl, O. Legrand, and F. Mortessagne, Fortschritte der Physik **61**, 404 (2013).
[64] H. Li, S. Suwunnarat, R. Fleischmann, H. Schanz, and T. Kottos, Phys. Rev. Lett. **118**, 044101 (2017).
[65] A. Grabsch, D. V. Savin, and C. Texier, Journal of Physics A: Mathematical and Theoretical **51**, 404001 (2018).
[66] P. del Hougne, D. V. Savin, O. Legrand, and U. Kuhl, Phys. Rev. E **102**, 010201 (2020).
[67] D. M. Pozar, *Microwave Engineering*, 4th ed. (John Wiley & Sons, 2011).
[68] E. Wilkinson, IRE Transactions on Microwave Theory and Techniques **8**, 116 (1960).